

WATER AT THE PHOENIX LANDING SITE

by

Peter Hollingsworth Smith

A Dissertation Submitted to the Faculty of the

COLLEGE OF OPTICAL SCIENCES

In Partial Fulfillment of the Requirements

For the Degree of

DOCTOR OF PHILOSOPHY

In the Graduate College

THE UNIVERSITY OF ARIZONA

2009

THE UNIVERSITY OF ARIZONA
GRADUATE COLLEGE

As members of the Dissertation Committee, we certify that we have read the dissertation

Prepared by Peter Hollingsworth Smith

Entitled Water at the Phoenix landing site

and recommend that it be accepted as fulfilling the dissertation requirement for the

Degree of Doctor of Philosophy

James C. Wyant Date: March 11th, 2009

Michael Drake Date: March 11th, 2009

Alfred McEwen Date: March 11th, 2009

William Hartmann Date: March 11th, 2009

William Boynton Date: March 11th, 2009

Final approval and acceptance of this dissertation is contingent upon the candidate's submission of the final copies of the dissertation to the Graduate College.

I hereby certify that I have read this dissertation prepared under my direction and recommend that it be accepted as fulfilling the dissertation requirement.

Dissertation Director: James C. Wyant Date: March 11th, 2009

Co-Dissertation Director: Michael Drake Date: March 11th, 2009

STATEMENT BY THE AUTHOR

This dissertation has been submitted in partial fulfillment of requirements for an advanced degree at The University of Arizona and is deposited in the University Library to be made available to borrowers under rules of the Library.

Brief quotations from this dissertation are allowable without special permission, provided that accurate acknowledgement of source is made. Requests for permission for extended quotation from or reproduction of this manuscript in whole or in part may be granted by the head of the major department or the Dean of the Graduate College when in his or her judgment the proposed use of the material is in the interest of scholarship. In all other instances, however, permission must be obtained by the author.

SIGNED: _____
Peter Hollingsworth Smith

ACKNOWLEDGMENTS

The Phoenix mission has performed exceptionally well due to the diligence of the Jet Propulsion Laboratory in partnership with the Lockheed Martin engineering team. The leadership of our project manager, B. Goldstein, has steered us away from unnecessary risk throughout the process. The University of Arizona provided the operations building and supported Phoenix throughout the mission. Special thanks to orbiter teams: in particular, the THEMIS (P. Christensen, PI) and the HiRISE (A. McEwen, PI).

I would also like to acknowledge the Phoenix Science Team who contributed greatly to this project: L.K. Tamppari, R.E. Arvidson, D. Bass, D. Blaney, W.V. Boynton, A. Carswell, D.C. Catling, B.C. Clark, T. Duck, E. DeJong, D. Fisher, W. Goetz, H.P. Gunnlaugsson, M.H. Hecht, V. Hipkin, J. Hoffman, S.F. Hviid, H.U. Keller, S.P. Kounaves, C.F. Lange, M.T. Lemmon, M.B. Madsen, M. Malin, W.J. Markiewicz, J. Marshall, C.P. McKay, M.T. Mellon, D.W. Ming, R.V. Morris, N. Renno, W.T. Pike, U. Staufer, C. Stoker, P. Taylor, J. Whiteway, and A.P. Zent.

Finally, this would never have happened without a loving and happy home environment provided by my darling wife, Dana Ann Smith.

DEDICATION

Dedicated to those I love most, my wife Dana Ann Smith and Sara H. Smith, my daughter.

TABLE OF CONTENTS

LIST OF FIGURES	7
ABSTRACT.....	9
CHAPTER 1 - INTRODUCTION.....	10
CHAPTER 2 - LOCAL GEOLOGY	11
CHAPTER 3 - EVIDENCE FOR AQUEOUS PROCESSES	24
CHAPTER 4 - INTERACTION OF SURFACE AND ATMOSPHERE.....	28
CHAPTER 5 - HABITABILITY	32
5.1 Energy sources for Life.....	33
5.2 Nutrients and Building Blocks.....	34
REFERENCES	36

LIST OF FIGURES

Figure 2-1 Geologic map showing the units surrounding the Phoenix landing site ⁷ . Ejecta deposits from the ~10 km Heimdal crater dominate the region surrounding the Lander. Differential eolian erosion of those deposits is also evident.	11
Figure 2-2 Sol 0 image of the patterned ground shaped by subsurface ice	13
Figure 2-3 Vertical projection of the panorama onto a plane 1.8 m below the camera level showing the digging area and beyond	14
Figure 2-4 The RA workspace topography with feature names	15
Figure 2-5 The ice table exposed by the thrusters named Holy Cow	16
Figure 2-6 The Snow Queen feature under the struts of the northeast footpad shows pits and fractures. The pebble tin the center may have been dislodged by the thruster blast. Note the spring in the upper left, part of the RA biobarrier...	17
Figure 2-7 The Dodo-Goldilocks trench matches high-albedo ice with a minor soil component compared with nearby ice-free soil exposed in the trench bottom (top). The spectra in the Snow White trench correspond to low albedo ice with a major soil component and nearby ice-free surface soil exposed in the trench bottom and to the sublimation lag developed 5 sols later at the same location as the ice (bottom).....	18
Figure 2-8 Snow White as seen under afternoon (left) and morning (right) illumination, showing freshly scraped hard material. Images were taken on sol 62 and 48 respectively).....	19
Figure 2-9 The Dodo-Goldilocks trench in afternoon Sun on sols 20 (left), 24 (center), and 62 (right). No digging was done during this time frame. Several 1.5-2.0 cm clods are visible in the shadow on sol 20 and missing on sol 24 indicating sublimation. By sol 62, the layer of white material had sublimated several mm, as indicated by the shadows at the left edge. The false color images are a uniform non-linear brightness stretch of 670-, 530-, and 440-nm images	20
Figure 2-10 OM images of Baby Bear sample on silicone substrate with 1 mm scale bar	20

Figure 2-11 OM image (2 mm high) of a sparse sample on the strong magnet. The rounded particles average to $\sim 150\ \mu\text{m}$ diameter, typical sizes for saltated grains.....	21
Figure 2-12 AFM scan showing 4 particles. The spheroidal particle in the center is $8\ \mu\text{m}$ in diameter, above it a plate-like particle is seen, the other two cross the boundary of the field.....	22
Figure 3-1 Endothermic peak observed by TEGA's thermal analyzer.....	24
Figure 3-2 Thermal and evolved water analysis for "Baby Bear" surface sample near Snow White. The mass-18 difference curve subtracts the second day reheat (sol 25) from the first temperature ramp (sol 22)	25
Figure 3-3 An enlargement of 3-2 showing the transition at 295°C	26
Figure 4-1 Atmospheric water vapor partial pressures measured by the TECP probe. Atmospheric values are within 2m of the ground with color-coding indicating solar longitude. Black circles are measurements made close to the surface in the regolith.	29
Figure 4-2 Nighttime image of surface frost from sol 80	30

ABSTRACT

The Phoenix mission investigated patterned ground and climate in the northern arctic region of Mars for 5 months starting May 25, 2008. A shallow ice table was uncovered by the robotic arm in a nearby polygon's edge and center at depths of 5-15 cm. In late summer snowfall and frost blanket the surface at night; water ice and vapor constantly interact with the soil. Analysis reveals an alkaline Ph with CaCO_3 , aqueous minerals, and salts making up several wt% of the soil; liquid water is implicated as having been important in creating these components. In combination with the oxidant perchlorate (~1 wt%), an energy source for terrestrial microbes, and a prior epoch of higher temperatures and humidity, this region may have been a habitable zone.

CHAPTER 1 - INTRODUCTION

The Phoenix mission, the first of NASA's Scout class, landed inside the arctic circle on Mars on May 25, 2008 at 23:38:24 UTC during the late northern Spring. At the first downlink opportunity the images showed a gently undulating landscape of patterned ground reminiscent of polar terrain on the Earth. Thus began a successful scientific investigation that lasted 152 sols (Martian days) and returned 30,000 images and other data related to the current climate, soil chemistry, and icy soil characteristics.

The mission and its goals have been previously described¹. Phoenix was designed to verify the presence of subsurface water ice that was predicted based on thermodynamic principles^{2,3} and was mapped within the upper meter of surface using Odyssey's Gamma Ray Spectrometer (GRS) instrument⁴. By analyzing the soil associated with the ice, Phoenix could learn the history of the ice and assess the habitability of the landing site. This paper addresses these two goals as well as the interaction of atmospheric water with the surface soil and ice.

CHAPTER 2 - LOCAL GEOLOGY

The Phoenix Lander touched down at 68.22° N, 234.25° E (areocentric) at an elevation of -4.1 km (referenced to Mars Orbiter Laser Altimeter areoid). The landing site is on a valley floor covered by the Scandia Formation, a deposit that surrounds the northern margin of a shield volcano named Alba Patera^{5,6}. The Scandia Formation is interpreted as volcanic ash associated with eruptions from Alba Patera and/or as fine-grained ancient polar deposits⁷. On a local scale the Lander touched down on partially eroded ejecta deposits located ~20 km from the rim of the 10 km diameter, bowl-shaped crater, Heimdal.

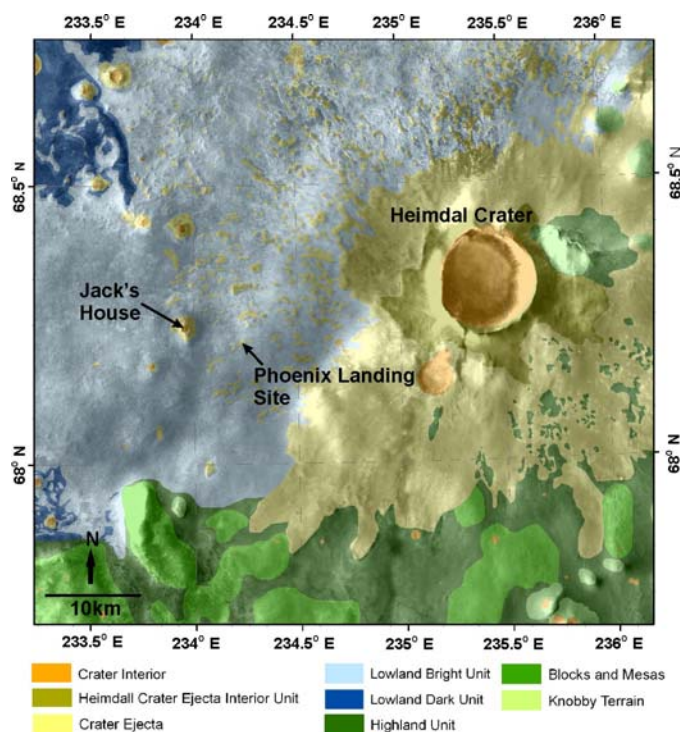


Figure 2-1 Geologic map showing the units surrounding the Phoenix landing site⁷. Ejecta deposits from the ~10 km Heimdal crater dominate the region surrounding the Lander. Differential eolian erosion of those deposits is also evident.

Based on counts of impact craters superimposed on its continuous ejecta deposit, Heimdal formed 0.5 to 0.75 Bya⁸. Crater counts for Scandia Formation surfaces not affected by emplacement of Heimdal ejecta indicate that these surfaces formed as early as 3 Bya. Aeolian stripping and icy soil sublimation loss of the Heimdal ejecta surfaces is evident within the vicinity of the Lander, leaving the original deposits as darker, rockier plateaus sitting ~1 m above lighter-toned plains. Phoenix landed on one of these darker surfaces and has the distinction of landing at the highest latitude on Mars and on the youngest terrain relative to the five other landed missions (two Viking Landers, Pathfinder, Spirit, and Opportunity).

The dominance of polygonal ground at the landing site is consistent with the presence of wide-spread, shallow, cohesive icy soil that has undergone seasonal or longer term cooling and cracking by elastic failure.

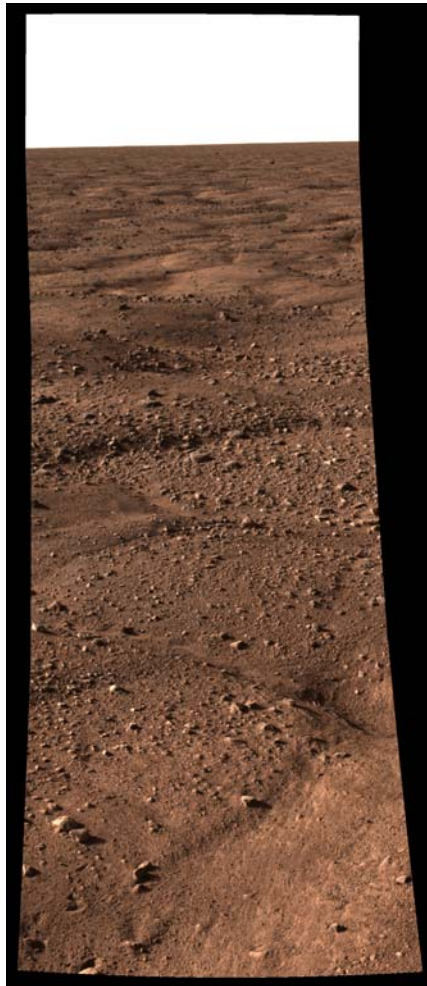


Figure 2-2 Sol 0 image of the patterned ground shaped by subsurface ice

After formation, the cracks filled with eolian sediments and when the icy soil warmed they were not able to close causing a slight upward bulging of the polygon interiors⁹. The troughs between the 2-3 m diameter polygons have typical depths of 20-50 cm relative to the centers. Small rocks are abundant and generally associated with troughs, but larger rocks (>1 m) are rare.

The 2.35 m long Robotic Arm (RA) and associated Icy Soil Acquisition Device (ISAD) have been used to excavate a dozen trenches within the RA work volume¹⁰. The

lander azimuth and lack of tilt gives the RA access to terrain between the north and northeast. A trough runs from the northwest under the north side of the Lander and at the near side of the workspace.

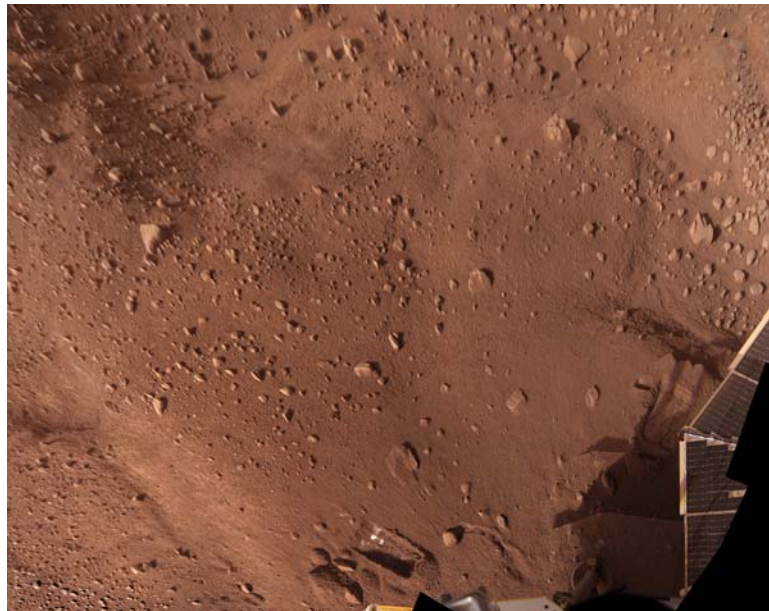


Figure 2-3 Vertical projection of the panorama onto a plane 1.8 m below the camera level showing the digging area and beyond

Six 10-20 cm diameter rocks are in the workspace along with many smaller pebbles. Two polygons are partly accessible, “Humpty Dumpty” to the north and “Wonderland” to the east, with the small trough, “Sleepy Hollow,” between them¹¹. Despite the low tilt, nearly 50 cm of topography is seen between the “Rabbit Hole” trough at the northwest side of the Lander to the “Wonderland” polygon in the east workspace.

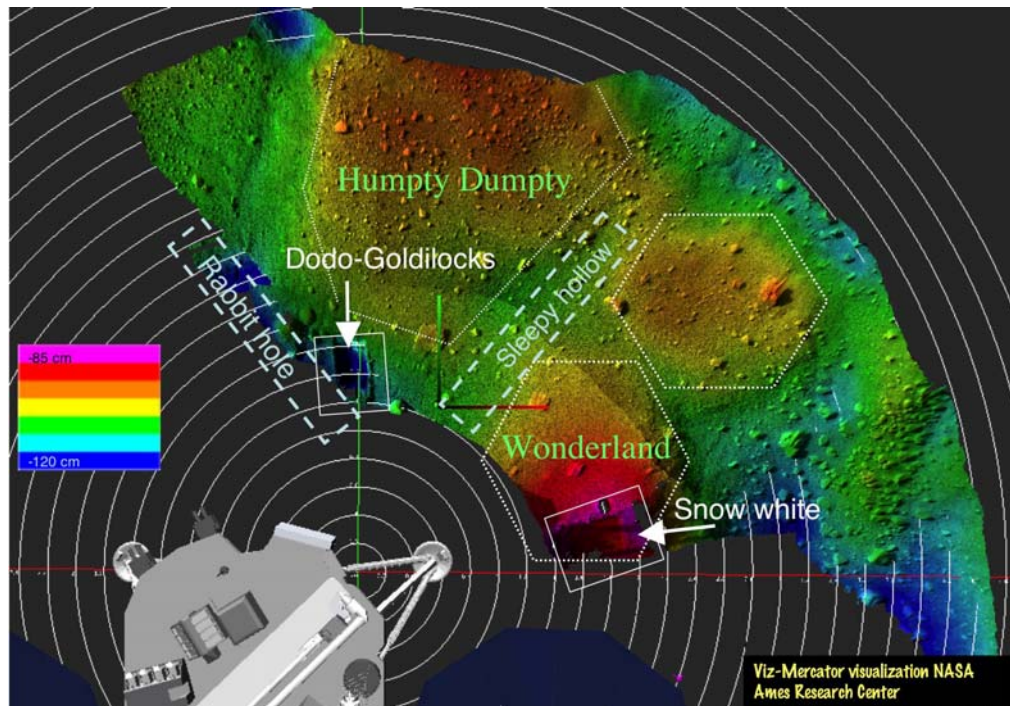


Figure 2-4 The RA workspace topography with feature names

All terrain visible to Surface Stereo Imager (SSI) prior to beginning RA activity was comprised of soil and dust coated rocks. However, Robotic Arm Camera (RAC) images under the Lander showed bright material exposed by the 12 thrusters during landing.

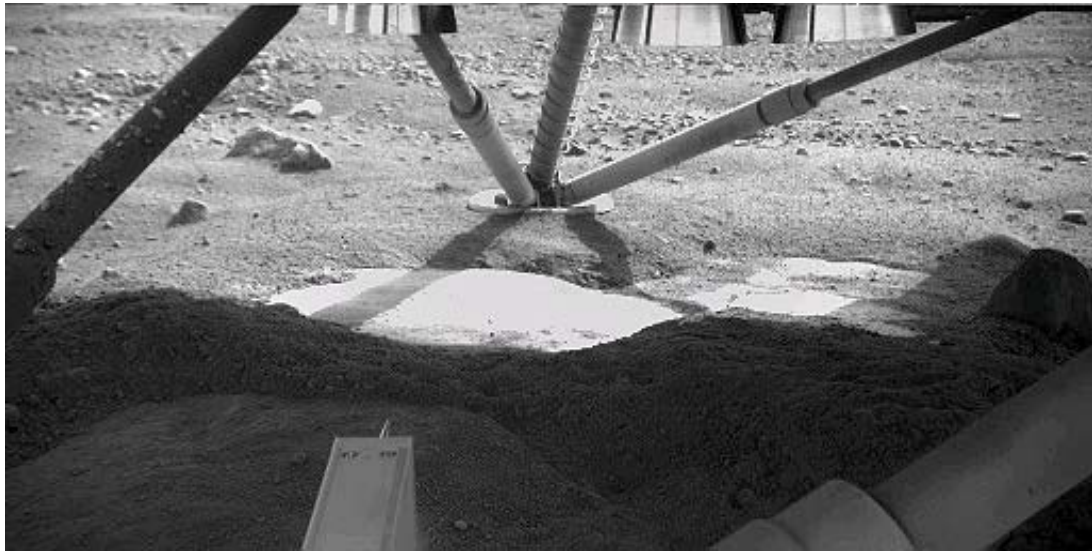


Figure 2-5 The ice table exposed by the thrusters named Holy Cow

Curved shadows from the leg struts across an exposure, “Holy Cow”, interior to the south leg imply a depth of about 5 cm below the undisturbed soil surface. An exposure, “Snow Queen”, under thrusters interior to the northeast landing leg was accessible for close (30-cm range) imaging throughout the mission. Late-mission images showed sublimation and fractures in the “Snow Queen” exposure.

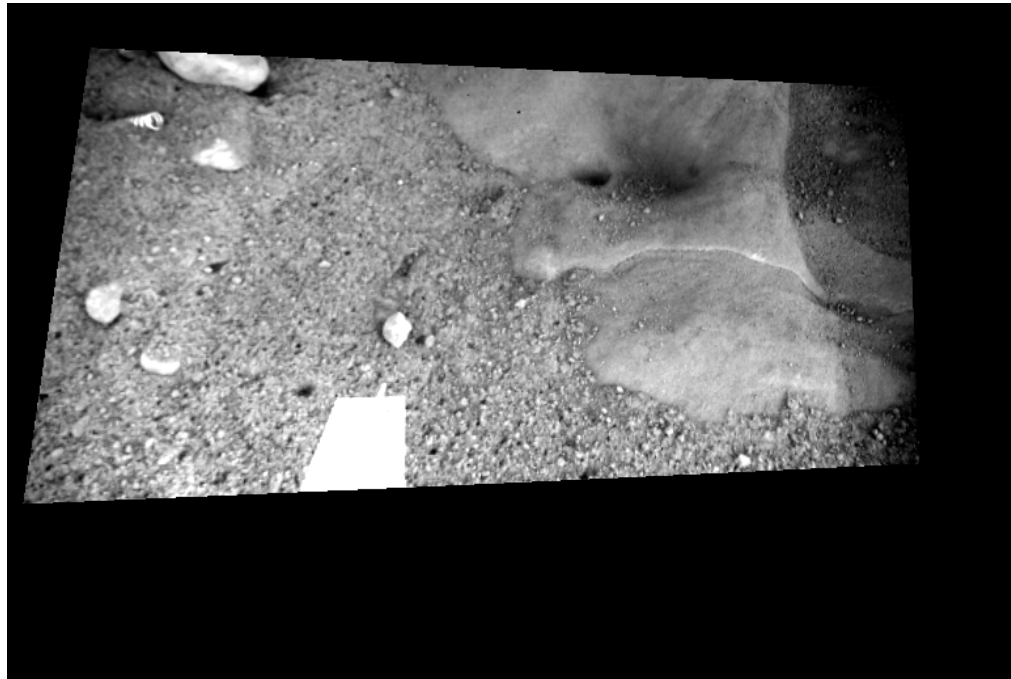


Figure 2-6 The Snow Queen feature under the struts of the northeast footpad shows pits and fractures. The pebble tin in the center may have been dislodged by the thruster blast. Note the spring in the upper left, part of the RA biobarrier.

Early RA operations uncovered hard, bright material in the Dodo-Goldilocks trench at a depth of 4-5 cm beneath soil, on the south side of Humpty Dumpty. SSI spectra show the bright material had a broad $\geq 1\text{-}\mu\text{m}$ absorption¹² and was bright in the blue filter ($<0.5\text{ }\mu\text{m}$) consistent with coarse-grained water ice with dust content of order a few percent.

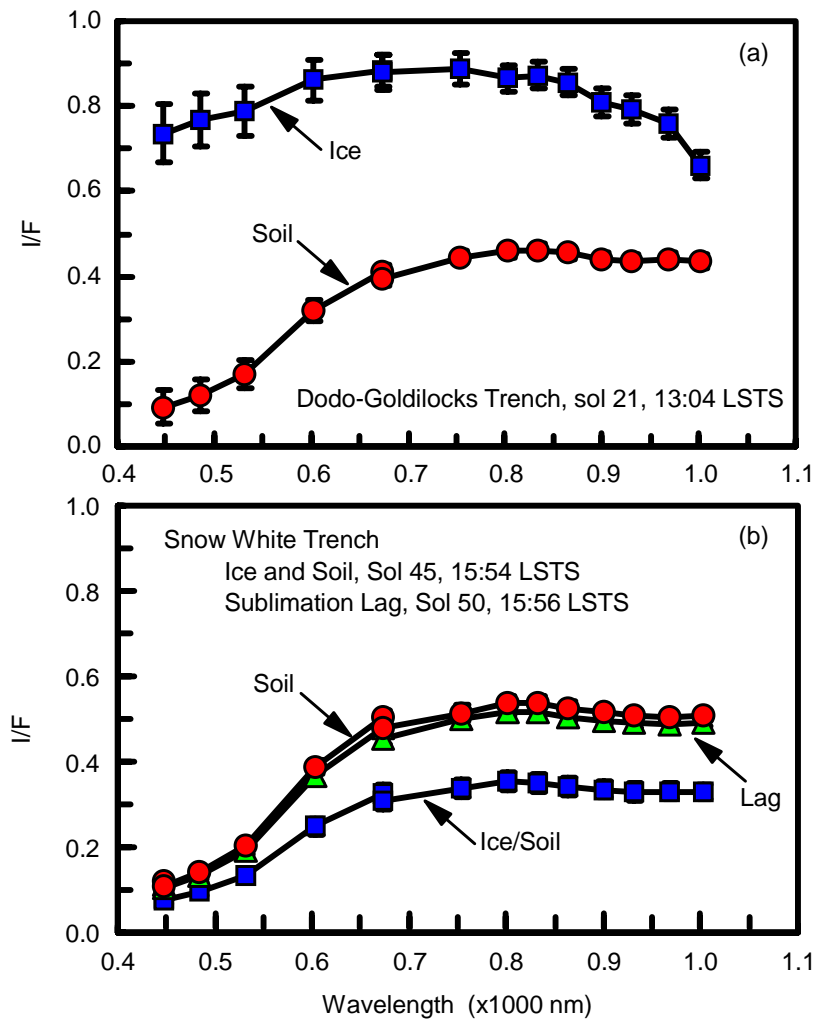


Figure 2-7 The Dodo-Goldilocks trench matches high-albedo ice with a minor soil component compared with nearby ice-free soil exposed in the trench bottom (top). The spectra in the Snow White trench correspond to low albedo ice with a major soil component and nearby ice-free surface soil exposed in the trench bottom and to the sublimation lag developed 5 sols later at the same location as the ice (bottom).

Not all trenches showed such a strong spectral contrast; in the Snow White trench the ISAD scraped into a hard, icy layer that appeared to be pore ice. Images of this trench in midday and early morning show variations in albedo.

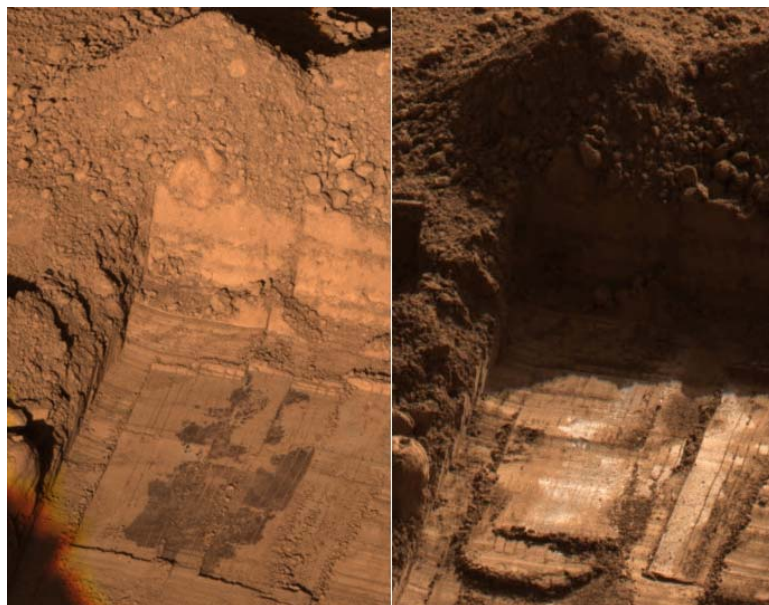


Figure 2-8 Snow White as seen under afternoon (left) and morning (right) illumination, showing freshly scraped hard material. Images were taken on sol 62 and 48 respectively).

On sol 20, several 1.5-2-cm chunks of bright material were dislodged by the RA and seen in the afternoon shadow of the trench wall. Lower quality images on sol 21 show the chunks still present, while images on sol 24 show no chunks and no obvious residue. No RA operations in the trench were conducted during this time. The spectral evidence and the observation that the sublimation timescale is 2-3 sols support the conclusion that the bright material is water ice. Over the next 2 months, the material was left undisturbed and the bright exposure was observed to sublimate several mm.



Figure 2-9 The Dodo-Goldilocks trench in afternoon Sun on sols 20 (left), 24 (center), and 62 (right). No digging was done during this time frame. Several 1.5-2.0 cm clods are visible in the shadow on sol 20 and missing on sol 24 indicating sublimation. By sol 62, the layer of white material had sublimated several mm, as indicated by the shadows at the left edge. The false color images are a uniform non-linear brightness stretch of 670-, 530-, and 440-nm images

An Optical Microscope (OM) image shows that the dominant materials in the samples are reddish fine-grained soils, forming agglomerates up to a few tens of μm across, as well as a small proportion ($<1\%$) of white particles of $20\ \mu\text{m}$ and below.

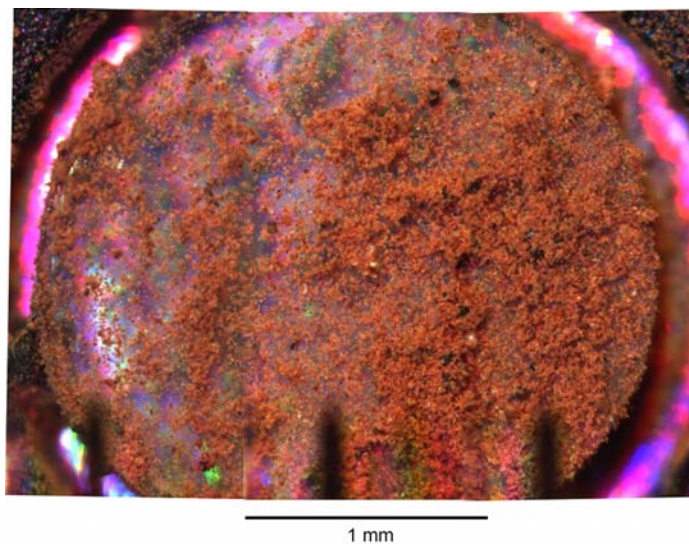


Figure 2-10 OM images of Baby Bear sample on silicone substrate with 1 mm scale bar

Additional soil components include magnetic 50-200 μm grains, mainly opaque black, brown, orange and yellow, with some translucent pale yellow. These larger particles are likely rounded by saltation. The time required for sample transfer would have prevented microscopic imaging of any ice particles prior to their sublimation.

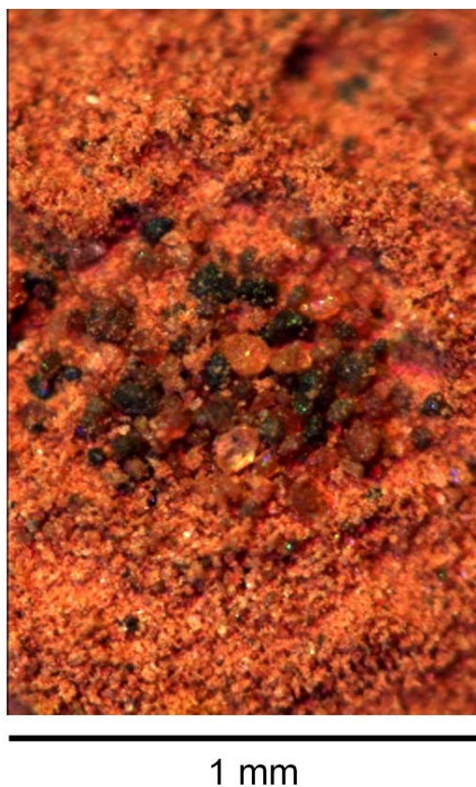


Figure 2-11 OM image (2 mm high) of a sparse sample on the strong magnet. The rounded particles average to $\sim 150 \mu\text{m}$ diameter, typical sizes for saltated grains

The Atomic Force Microscope (AFM) imaged the fines at higher resolution, producing scans of a variety of particles often with a platy morphology.

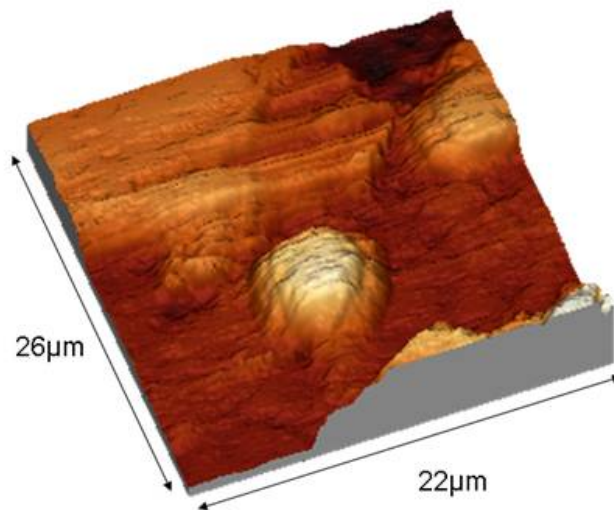


Figure 2-12 AFM scan showing 4 particles. The spheroidal particle in the center is 8 µm in diameter, above it a plate-like particle is seen, the other two cross the boundary of the field

The soil is likely partially weathered material of aeolian origin dominated by agglomerates of primarily reddish particles, with a minor proportion of strongly magnetic, silt-to-sand-sized grains with the fine, non-magnetic white particles interpreted as salt. The soils excavated by the ISAD are cloddy, with mechanical properties similar to those found for cloddy soils sampled by the Viking Lander 2¹³. No ripples or dunes are seen at the site and the landscape seems degradational: dust devils scour the surface. Certainly, the crust that produces the clods formed in place. The larger particles in the soil, 50-200 µm in diameter, have not saltated long distances although the clay-sized particles have almost certainly been transported a considerable distance by the winds. In summary, Phoenix detected water ice in situ for the first time on Mars. The ice table first seen under the lander exposed by the thrusters is measured to be from 3-15 cm deep from polygon center to trough. Phoenix has revealed two types of ice: an exposed matrix

of nearly pure ice in Dodo-Goldilocks and soil-pore ice in Snow White. Pore ice has been predicted by thermodynamical arguments¹⁴, but the exposure of nearly pure ice is hard to explain and may in fact support the Odyssey GRS conclusion that ice concentrations must be greater than pore ice to explain the large ice signals¹⁵.

CHAPTER 3 - EVIDENCE FOR AQUEOUS PROCESSES

Attempts to collect and to deliver ice-cemented soil materials to the Thermal and Evolved Gas Analyzer (TEGA) ovens were not successful; therefore, a sample of the sublimation till material at the bottom of the Snow White Trench was collected by the RA scoop on sol 63. A small, endothermic peak was observed by TEGA's thermal analyzer. The differential power illustrates the endothermic peak for the melting of water ice with an onset temperature at -2°C and a peak around 6°C. Evolved water was recorded by TEGA's mass spectrometer as the temperature increased from -20 to +35°C.

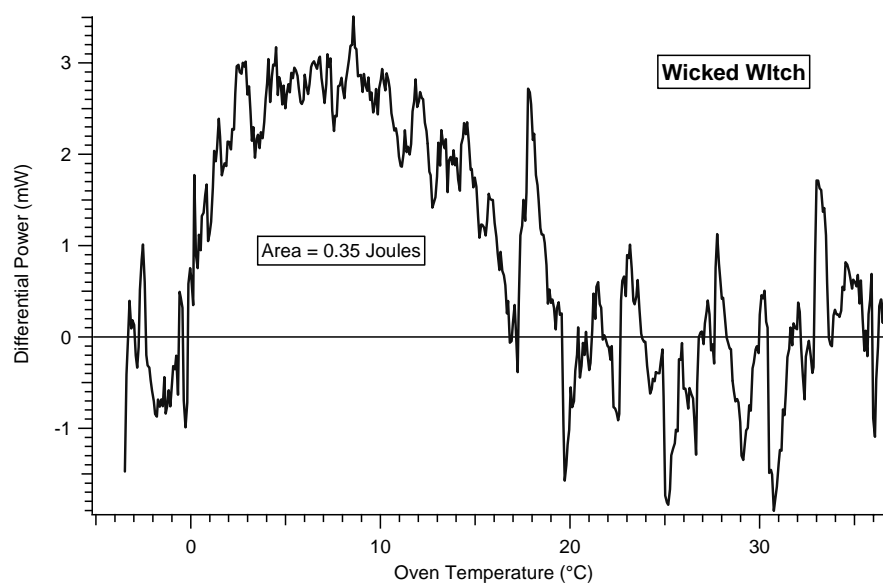


Figure 3-1 Endothermic peak observed by TEGA's thermal analyzer

The endothermic peak and evolution of water indicate a small amount of water ice in the sample named "Wicked Witch." Integration of the endothermic peak provides an

estimate of the enthalpy of 0.35 J, which corresponds to 1.04 mg of water ice (latent heat of fusion of ice is 333 J/g). Assuming a full TEGA oven, the ice content of the sample is estimated at 2%. Because this sample was from sublimation lag, this does not represent the ice concentration in the ice layer.

Although TEGA analysis is not definitive for mineralogy, important constraints can be inferred by analyzing the evolved gas. Two temperature regions of water release for a surface sample taken just west of the Snow White trench dubbed “Baby Bear” are shown in Figure 3-2 and 3-3.

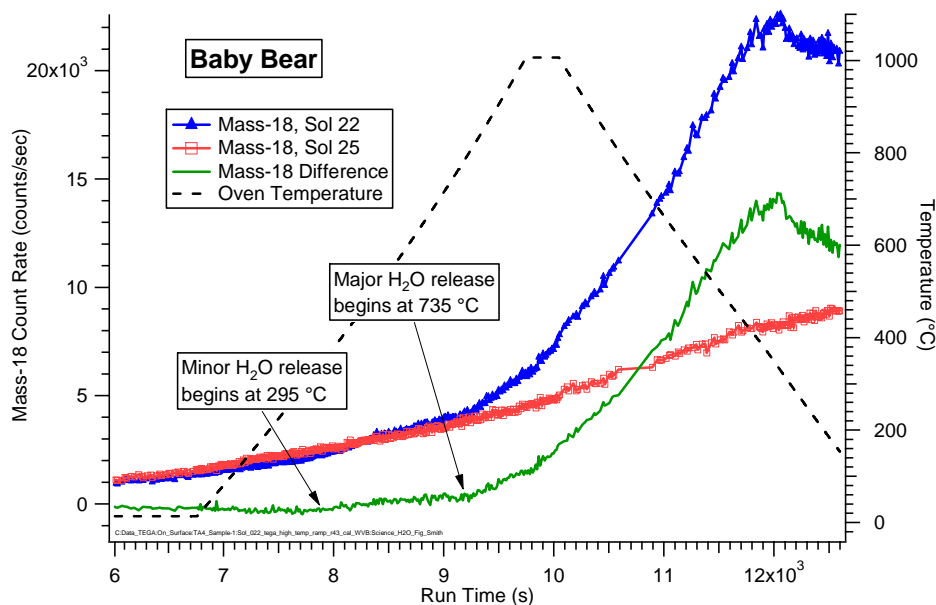


Figure 3-2 Thermal and evolved water analysis for “Baby Bear” surface sample near Snow White. The mass-18 difference curve subtracts the second day reheat (sol 25) from the first temperature ramp (sol 22)

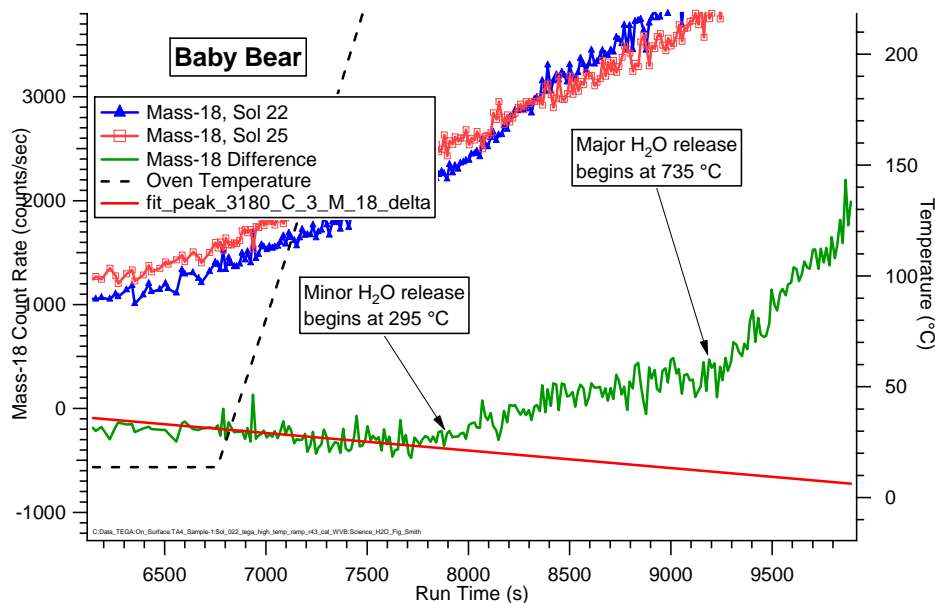


Figure 3-3 An enlargement of 3-2 showing the transition at 295°C.

A “low” temperature water release begins around 295°C continuing to 735°C, this can result from a variety of phases¹⁶. The important implication of this lower temperature water release is that the group of minerals or phases that are candidates can only form by aqueous processes.

The “high” temperature water release beginning near 735°C also may be due to a variety of candidate phases¹⁷. Formation processes for these candidates may be aqueous and non-aqueous; non-aqueous processes may include igneous or metamorphic processes. Even so, water must have been associated with the magma body or a precursor material, respectively.

The diffusion of water vapor into and out of the regolith during diurnal and seasonal changes may activate unfrozen “films” of water around soil particles¹⁸. The

Thermal and Electrical Conductivity Probe (TECP) electrical conductivity measurements endeavored to measure these films, but were consistent with a fully open circuit, implying that there is no effective transport of charge carriers on the scale of the TECP tines (15 mm). Nighttime increases in regolith dielectric permittivity, observed during the latter half of the mission (mid to late summer), are consistent with an overnight accumulation of H₂O molecules in the regolith. Furthermore, at high obliquity, when summertime insolation to both the regolith and the nearby polar cap is at a maximum, thicker films are likely: a key unknown is the persistence of high latitude surface ice¹⁹.

The loose soil has no measurable water or ice in the current epoch during the summer season, although a small amount of adsorbed or volumetrically bound water is implied by the 3- μ m band seen from the OMEGA and CRISM orbiting spectrometers. Orbital and obliquity variations over the last 10 Mya offer opportunities for large releases of water from the ice cap with snow deposited at the Phoenix site. Warmer temperatures may lead to wetting of the soil. The cloddy nature of the soil may be a consequence of cementation associated with carbonates or other cementing agents and a small amount of water. Indeed, compounds normally formed in liquid water are found in the samples analyzed by TEGA. The Phoenix discovery of Ca-carbonate²⁰ and minerals that release water at low temperatures argue for a past when the soil was moist.

CHAPTER 4 - INTERACTION OF SURFACE AND ATMOSPHERE

Phoenix made near continuous measurements of air temperature at 0.25, 0.50 and 1.00 m above the ~1 m high instrument deck and of air pressure at deck level²¹. The 1-m sensor shows a regular diurnal cycle with maxima between -30 and -20°C in the early afternoon, and minima of about -80°C between 1:00 and 2:00 LST (Local Solar Time). By the end of the mission the temperature minima dropped to below -95°C. Pressure decreased from ~855 Pa on Sol 5 (L_s 78°, L_s =Solar longitude) to a seasonal minimum of ~725 Pa on Sol 140 (L_s 142°). These pressures are above the triple point of water, 610 Pa, but temperatures must rise above 0°C for pure liquid water to form. In addition, hundreds of pressure perturbations of order 1 Pa, probably caused by convective vortices, were observed as sharp dips in pressure occurring over a time interval of about 30 s, usually in the early afternoon.

Atmospheric water vapor was measured regularly near the surface using the TECP. These measurements indicated that the water vapor partial pressure maintained a value near 2 Pa throughout the day dropping rapidly at 18:00 LST to a minimum of <0.05 at 1:30 LST.

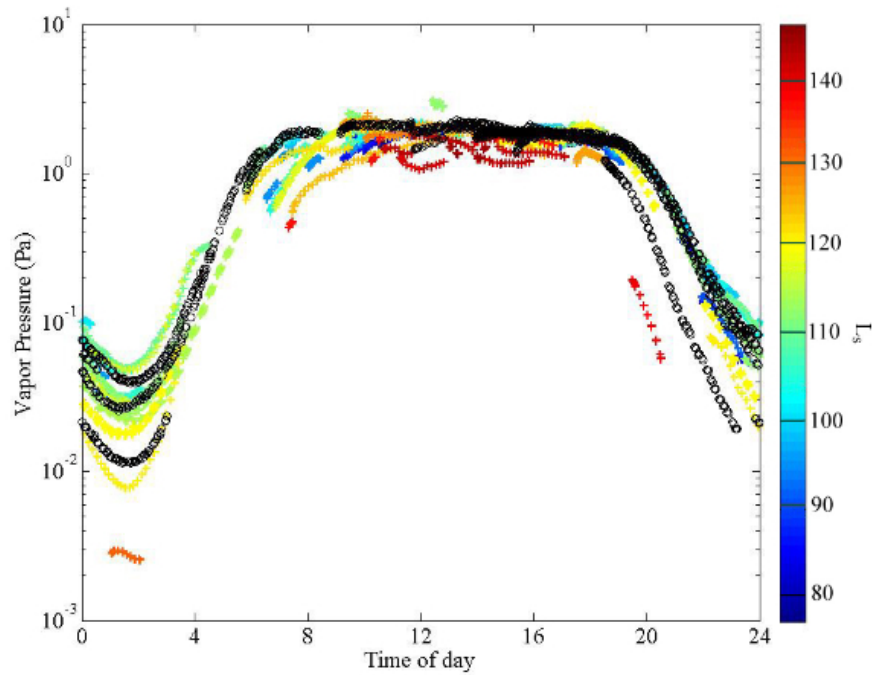


Figure 4-1 Atmospheric water vapor partial pressures measured by the TECP probe. Atmospheric values are within 2m of the ground with color-coding indicating solar longitude. Black circles are measurements made close to the surface in the regolith.

Vapor pressure of 2 Pa is approximately that of saturation over ice at -55°C . The water vapor measurements and 2-m air temperatures suggest that the typical mid-sol relative humidity was $\sim 5\%$. The air was close to saturation at night early in the mission and was saturated towards the end of the mission as seen via fog and low clouds. Surface temperatures are expected to be colder than those measured at 2 m and indeed frost formation was observed in the second half of the mission.

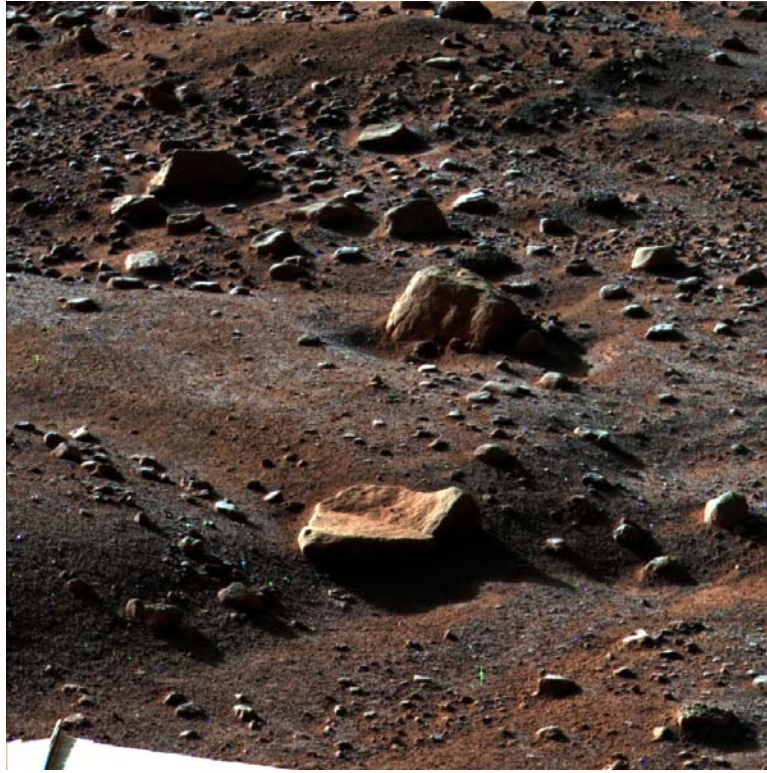


Figure 4-2 Nighttime image of surface frost from sol 80

The LIDAR experiment²² measured clouds and dust in the atmosphere and the height of the mixed layer. For the first 80 sols, the LIDAR mainly observed atmospheric dust. The turbulent boundary layer was observed to be 4 to 5 km deep, with a peak height in the late afternoon. Dust loading of the atmosphere decreased through the mission and after sol 100 the extinction coefficient due to dust was less than half what it was near summer solstice (sol 30).

Water ice clouds were detected by the LIDAR as layers of enhanced signal. Near summer solstice the most prominent clouds were detected at heights above 10 km. As the season progressed and the polar atmosphere cooled, clouds formed in the boundary layer in late summer (after $L_s = 117^\circ$) and fall streaks are clearly seen in the LIDAR

observations²³. As shown in Figure 4-2, water ice is observed to fall from the clouds at 4 km altitude; ground fogs are seen late at night in the lower ~700 m of atmosphere (20), and frost forms early in the morning. Figure 4-1 shows this diurnal cycle deposits ice onto the surface at night reducing the humidity to low values, sublimates it in the morning, and redistributes it throughout the planetary boundary layer in the turbulent afternoon. Eventually ice clouds form that precipitate the ice back to the surface late at night. These tiny grains of ice could melt if temperatures were warmer and frost thicker during a different climate cycle or in warmer microclimates.

CHAPTER 5 - HABITABILITY

An important mission goal was to evaluate the biological potential of the high-latitude ice-rich region of Mars. According to Mars mission planning studies²⁴ the potential for habitability in a specific time and space encompasses three factors: (1) the presence of liquid water, (2) the presence of a biologically available energy source, and (3) the presence of the chemical building blocks of life (e.g. C, H, N, O, P, S) in a biologically available form.

Drawing from experience with terrestrial extremophiles, there are boundaries below which life is not viable. Two important conditions need to be met before life can metabolize, grow, and reproduce: the temperatures must exceed -20°C on the average and the water activity (a_w) level must be >0.50 (24,25). For Martian conditions, this implies that at a temperature of -20°C the partial pressure of water above an ice layer must exceed 50 Pa ²⁶.

This is difficult to achieve for long periods of time. Figure 4-1 shows that the Phoenix measured value is $<2\text{ Pa}$ during midday with extremely low values at night. As temperatures slowly warm during climate change, the ice table quickly adjusts by subliming to a deeper, colder level. Quasi-periodic changes in solar insolation occur in the North polar region as a result of orbital dynamics and obliquity changes²⁷. In the current epoch, northern summer occurs during aphelion, and obliquity is 25.2° . Perihelion longitude precesses with a 51,000-year cycle and when northern summer

corresponds with perihelion, summer surface temperatures are predicted to exceed 0°C several days each year²⁸. As the obliquity exceeds 30° , the polar cap becomes unstable and releases water vapor into the atmosphere saturating it and forming ice clouds. Over the last 10 Ma maximum obliquity approached 45° and increased the local summer insolation to approximately twice the present value. Under those conditions the surface temperature may exceed 0°C for 100 days per year²⁸ and a moisture-laden boundary layer may emplace a deep enough layer of frost or snow during the cold nighttime that it would survive to the midday and partially melt into the soil. Thus the local partial pressure of water and the activity level may exceed the minimum conditions for metabolism.

5.1 Energy sources for Life

Sunlight is the most available form of energy and the surface environment might be habitable given sufficient liquid water, but ionizing UV radiation would be a significant challenge for life. In the subsurface, chemical energy would be needed to support metabolism.

Perchlorate salt was identified in the soil by WCL, probably in the form of $\text{Mg}(\text{ClO}_4)_2$ ²⁹. The reduction potential of perchlorate and chlorate (1.287V; 1.03V, respectively) makes them ideal electron acceptors for microbial metabolism³⁰ and these compounds are known to be utilized as an energy source by numerous species of microbes³¹. These bacteria obtain energy for growth by the oxidation of organic carbon or inorganic electron donors (e.g., H_2 , H_2S , or Fe^{++}) coupled to the reduction of perchlorate. Perchlorate-reducing microbes, identified from numerous soil and sediment

environments³², can grow under a wide range of environmental conditions, and have a broad range of metabolic capabilities including the oxidation of soluble and insoluble ferrous iron^{33,34,35}. The most common genera of organisms that perform perchlorate reduction (*Dechloromonas* and *Azospira*) have been found in Mars analog environments, including Antarctic soils³⁶. However, the other half of the redox couple has not been identified.

5.2 Nutrients and Building Blocks

C and H are present in the readily useable forms of CO₂ and H₂O in the Martian environment. The measured pH of ~8.3¹⁴ is slightly alkaline, comparable to most semiarid soils, and ideal for a broad range of organisms. Alkaline solutions, unlike strongly acid ones inferred from Mars rover results, do not preclude the sort of prebiotic chemistry generally considered necessary for the origin of life³⁷. WCL has also measured ions of Ca, Cl, K, Na, and Mg, all recognized as nutrients for microbial growth that are within the normal range of variability for terrestrial soils. Phoenix instruments are not sensitive to nitrates in the presence of perchlorate or phosphates in the soil and No sulfates have been detected implying an insoluble form since sulfur is an expected component of the dust.

While Phoenix did not prove that the environment is habitable, the modern environment of the Phoenix landing site has many and possibly all of the characteristics that would have been needed to support life in the geologically recent past. With the present parameters of obliquity and perihelion longitude, liquid water is possible only in

thin films or brines, but in previous epochs of higher obliquity temperatures were warmer and therefore liquid formation was more likely. Given liquid water formation, energy and nutrients are available to support life.

REFERENCES

1. P. H. Smith et al., *J. Geophys. Res.* **113**, E00A18, doi:10.1029/2008JE003083 (2008).
2. M. T. Mellon and B. M. Jakosky, *J. Geophys. Res.*, **100**, 11781-11799 (1995).
3. R. B. Leighton and B. C. Murray, *Science* **153**, 136 (1966).
4. I. G. Mitrofanov et al., *Science* **300**, 2081-4 (2003).
5. R. E. Arvidson et al., *J. Geophys. Res.* **113** E00A03 (2008).
6. K. L. Tanaka, Skinner, J. A., Jr., and Hare, T. M., USGS Sci. Inv. Map (SIM) 2888, (2008).
7. K. Seelos et al., *J. Geophys. Res.* **113**, E00A13 (2008).
8. W. K. Hartmann and G. Neukum, *Space Sci. Rev.* **96**, 165-194 (2001)).
9. M. T. Mellon et al., *J. Geophys. Res.* **113**, E00A23 (2008).
10. R. Bonitz et al., *J. Geophys. Res.* **113**, E00A01 (2008).
11. The mission adopted the convention that features around the lander were generally (though not strictly) named after fairy tales. The lander azimuth was controlled during landing to within a degree keeping the workspace shaded in the afternoon and the tilt was 0.3° to the west.
12. The band was deepest at 1 μ m, but no longer wavelength filters were available.
13. H. Moore et al. U.S.G.S. Prof. Paper 1389 (1987).
14. M. T. Mellon et al., *J. Geophys. Res.* **113**, E00A25 (2008).
15. W. C. Feldman, M. T. Mellon, O. Gasnault, B. Diez, R. C. Elphic, J. J. Hagerty, D. J. Lawrence, S. Maurice, & T. H. Prettyman, *Geophys. Res. Lett.* **34**, L05201, doi:10.1029/2006GL028936 (2007).
16. Candidate phases for “low” temperature (295-735°C) release of water include Fe-oxyhydroxides (e.g., goethite dehydroxylation onset around 250°C), smectites (e.g., nontronite dehydroxylation onset around 300°C), kaolinite (dehydroxylation onset 400-550°C depending on crystallinity), Fe-sulfates (e.g., jarosite dehydroxylation onset near 400°C), Mg-sulfates (e.g. kieserite loss of crystalline water near 350°C), basaltic glass (loss of occluded water near 400°C) and other potential phases.

17. The “high” temperature water release starting around 735°C may be due to the presence of smectites (e.g., montmorillonite dehydroxylation from 600-800°C, saponite dehydroxylation near 700-800°C), chlorites, talc (dehydroxylation from 750-850°C), serpentines (e.g., antigorite dehydroxylation from 600-800°C), and other potential phases.
18. A. Zent, *Icarus* **196**, 385–408 (2008).
19. B. M. Jakosky and M. H. Carr, *Nature* **315**, 559-561 (1986). Head, J. W., J. F. Mustard, M. A. Kreslavsky, R. E. Milliken, and D. R. Marchant, *Nature* **426**, 797 – 802 (2003).
20. W. V. Boynton et al., *Science*, this issue (2009).
21. P. A. Taylor, D. C. Catling, M. Daly, C. S. Dickinson, H. P. Gunnlaugsson, A. Harri, and C. F. Lange, *J. Geophys. Res.* **113**, E00A10, doi:10.1029 /2007JE003015 (2008).
22. J. Whiteway, M. Daly, A. Carswell, T. Duck, C. Dickinson, L. Komguem, and C. Cook, *J. Geophys. Res.* **113**, E00A08, doi:10.1029/2007JE003002 (2008).
23. J. Whiteway et al. *Science*, this issue (2009).
24. D. W. Beatty et al., Findings of the SR-AG, white paper, 76 p. at <http://mepag.jpl.nasa.gov/reports/index.html> (2006).
25. W.D. Grant, *Phil. Trans. of the Roy. Soc. of London*, 1249-1267 (2004).
26. J. Marti and K. Mauersberger, *Geophys. Res. Lett.* **20**, 363-6 (1993). A. L. Buck, *J. Appl. Meteorol.* **20**, 1527-32 (1981).
27. J. A. Laskar, C. M., Correia, M. Gastineau, F. Joutel, B. Levrard, & P. Robutel, *Icarus* **170**, 343-364 (2004).
28. M. I. Richardson and M.A. Mischna, *J. Geophys. Res.* **110**, E03003, 2004JE002367 (2005).
29. M. Hecht et al., *Science*, this issue (2009).
30. J. D. Coates, U. Michaelidou, S. M. O’Connor, R. A. Bruce, & L. A. Achenbach in *Perchlorate in the Environment* (ed. Urbansky, E. T.) 257–270 (Kluwer Academic/Plenum, New York) (2000).
31. J. D. Coates and L. A. Achenbach, *Nature Rev. Microbiology* **2**, 569-580 (2004).
32. W. Wallace, T. Ward, A. Breen, & H. Attaway, *J. Ind. Microbiol.* **16**, 68–72 (1996).
33. J. D. Coates et al., *Appl. Environ. Microbiol.* **65**, 5234–5241 (1999).

34. R. A. Bruce, L. A. Achenbach, & J. D. Coates, *Environ. Microbiol.* **1**, 319–331 (1999).
35. U. Michaelidou, L. A. Achenbach, & J. D. Coates in *Perchlorate in the Environment* (ed. Urbansky, E. T.) 271–283 (Kluwer Academic/Plenum, New York) (2000).
36. K. S. Bender, M. R. Rice, W. H. Fugate, J. D. Coates, and L.A. Achenbach, *Appl. Envir. Microbiol.* **70**, 5651-5658 (2004).
37. A.H. Knoll et al., *Earth Planet. Sci. Lett.* **240**, 179-189 (2005).